Characterization of chaotic electroconvection near flat electrodes under oscillatory voltages

By J. Kim, S. Davidson AND A. Mani

1. Motivation and objectives

Above certain critical voltages, electrokinetic systems under external electric fields exhibit electroconvective instability, where ion transport and hydrodynamics are closely coupled. Strong electric fields applied across charge-selective interfaces drive concentration polarization and cause severe ion depletion near the interface. Additionally, the screening electric double layer (EDL) makes a transition to a non-equilibrium structure with the formation of the extended space charge layer, which is prone to transverse instabilities (Zaltzman & Rubinstein 2007). Typically, arrays of coherent vortical structures emerge near charge-selective surfaces, and broadbanded energy spectra are observed (Rubinstein *et al.* 2008; Druzgalski *et al.* 2013; Davidson *et al.* 2014). As applied voltage increases, the system becomes more irregular in its response and eventually makes a transition to fully chaotic states (Druzgalski *et al.* 2013; Demekhin *et al.* 2013; Davidson *et al.* 2014). Investigation of such regimes requires a fully nonlinear analysis such as direct numerical simulation of fully coupled Poisson–Nernst–Planck and Stokes equations (Demekhin *et al.* 2011; Pham *et al.* 2012; Druzgalski *et al.* 2013; Druzgalski & Mani 2016). Summaries of recent advances in the understanding of electroconvective instability in various applications are given by Chang *et al.* (2012) and Nikonenko *et al.* (2014, 2016, 2017).

One characteristic feature of electroconvective instability is increased mixing, facilitated by arrays of large-scale vortices. Recent studies have provided important evidence that enhanced hydrodynamic mixing is well correlated with overlimiting current measured at high applied voltages (Rubinstein *et al.* 1988, 2008; de Valença *et al.* 2015). This link calls for further studies on understanding and characterizing electroconvective flows so that the controllability and efficiency of practical electrokinetic systems such as fuel cells, water desalination, electrodialysis, micropumps and flow mixers can be significantly improved.

All of the theoretical investigations of electroconvection consider systems under direct current (DC) electric forcing, and most often with ion-selective membranes as the ion exchange interface. In this study however, we explore existence and regimes of electroconvection in alternating current (AC) setups and near flat electrodes. An external oscillatory timescale, imposed on top of intrinsic ones such as the charge-relaxation time and the resistorcapacitor (RC) charging timescale (Bazant *et al.* 2004), complicates the mechanisms of hydrodynamic coupling with ion transport and the overall system level responses. How such a system can be characterized in the context of electroconvective instability and mixing enhancement remains largely unexplored. One-dimensional theories and extensive discussions of AC electro-osmosis, particularly in weakly and strongly nonlinear regimes, can be found in the literature (Suh & Kang 2008; Olesen *et al.* 2010; Schnitzer & Yariv 2014; Stout & Khair 2015).

This study investigates the onset of electroconvective instability in an electrokinetic

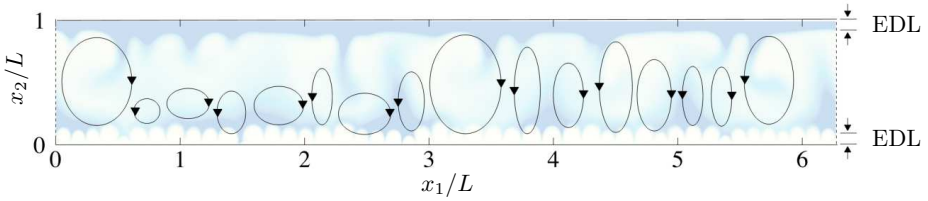

FIGURE 1. Computational domain. Also shown are schematics of large-scale vorticies and electric double layers (EDLs) near AC electrodes at $x_2/L = 0$ and 1 (not to scale). The domain is periodic in the x_1 direction.

system subject to oscillatory voltages. A two-dimensional aqueous binary electrolyte bounded by two flat electrodes is considered, and an external AC electric field at a single oscillation frequency is applied in the wall-normal direction. We show that at sufficiently high voltages (in units of thermal volts, defined in Section 2), electroconvective instability is triggered and sustained. In particular, the AC oscillation frequency and diffusivity ratio of ionic species are assessed for their impacts on the development of electroconvective instability.

This report is organized as follows: The computational setup is given in Section 2, followed by a description of a fully conservative numerical scheme used to solve governing equations in Section 3. A detailed characterization of electroconvective instability is presented in Section 4. Conclusions and suggested future works are discussed in Section 5.

2. Problem setup

The governing equations and physical parameters are similar to those of Druzgalski *et al.* (2013) and Davidson *et al.* (2014, 2016), who studied electroconvective instabilities under moderate DC electric fields. Transport of ionic species in an aqueous binary electrolyte under applied voltages is modeled by the two-dimensional Poisson–Nernst–Planck equations in a dilute limit. As shown in Figure 1, a two-dimensional channel of aspect ratio 2π is considered with its top and bottom walls corresponding to ideally polarizable electrodes with zero Faradaic current. Throughout this report, x_1 and x_2 denote the horizontal and wall-normal directions, respectively. Within the channel, concentration (or number density) of cations (c^+) and anions (c^-) having the same valence, $z = 1$, is solved for. Superscripts + and − are used to denote quantities of cations and anions, respectively. Thermal equilibrium at room temperature is assumed, and molecular diffusivity D for each species is uniform in space and constant in time. However, diffusivity is allowed to vary from one species to another. The Nernst–Planck equation for ionic transport is written as

$$\frac{\partial c^{\pm}}{\partial t} + \boldsymbol{u} \cdot \boldsymbol{\nabla} c^{\pm} = \boldsymbol{\nabla} \cdot (D^{\pm} \boldsymbol{\nabla} c^{\pm}) \pm \boldsymbol{\nabla} \cdot \left(D^{\pm} \frac{1}{V_T} c^{\pm} \boldsymbol{\nabla} \phi \right), \tag{2.1}$$

where $\boldsymbol{u} = \{u_1, u_2\}$ is flow velocity, $V_T = k_B T/(ze)$ is the thermal voltage with k_B, T and e being the Boltzmann constant (1.38×10^{-23} J/K), absolute temperature and the elementary charge (1.6×10^{-19} C), respectively, and ϕ is the electric potential. This is coupled with Gauss's law

$$\boldsymbol{\nabla}^2 \phi = -\frac{\rho_e}{\varepsilon}, \tag{2.2}$$

where $\rho_e = ze(c^+ - c^-)$ is the charge density and ε is the electrical permittivity.

Hydrodynamic transport is evaluated by solving the Navier–Stokes equations at the incompressible, low-Reynolds limit. Thus, the nonlinear convection term is neglected. Instead, an electrohydrodynamic coupling term is included in the momentum equations.

$$\boldsymbol{\nabla}\cdot\boldsymbol{u}=0, \tag{2.3}$$

$$\rho\frac{\partial \boldsymbol{u}}{\partial t}=-\boldsymbol{\nabla}p+\boldsymbol{\nabla}\cdot(\mu\boldsymbol{\nabla}\boldsymbol{u})-\rho_{\mathrm{e}}\boldsymbol{\nabla}\phi, \tag{2.4}$$

where ρ is density, p is static pressure and μ is dynamic viscosity. Due to the thermal equilibrium assumption, all thermodynamic quantities in this study are uniform.

Equations (2.1)-(2.4) are nondimensionalized by relevant reference quantities such as the channel height L (see Figure 1) for length, D^+ for molecular diffusivity, L^2/D^+ for time, D^+/L for velocity, initial average salt concentration c_0 for ion concentration, the osmotic pressure $\mu D^+/L^2$ for pressure and V_T for electric potential. As a result, six dimensionless parameters characterize the electrohydrodynamics of the given system, namely the electrohydrodynamic coupling constant $\kappa=\varepsilon V_T^2/(\mu D^+)$, nondimensional Debye–Hückel screening length $\epsilon=\lambda_{\mathrm{D}}/L$, Schmidt number $\mathrm{Sc}=\mu/(\rho D^+)$, nondimensional maximum voltage $\Delta V=V_{\max}/V_T$, nondimensional oscillation frequency ω and the ratio of diffusivities D^-/D^+. The Debye screening length is defined by

$$\lambda_{\mathrm{D}}=\sqrt{\frac{\varepsilon k_B T}{2(ze)^2 c_0}}. \tag{2.5}$$

The nondimensional governing equations are

$$\frac{\partial \widetilde{c}^{\pm}}{\partial \widetilde{t}}+\widetilde{\boldsymbol{u}}\cdot\widetilde{\boldsymbol{\nabla}}\widetilde{c}^{\pm}=\widetilde{\boldsymbol{\nabla}}\cdot(\widetilde{D}^{\pm}\widetilde{\boldsymbol{\nabla}}\widetilde{c}^{\pm})\pm\widetilde{\boldsymbol{\nabla}}\cdot\left(\widetilde{D}^{\pm}\widetilde{c}^{\pm}\widetilde{\boldsymbol{\nabla}}\widetilde{\phi}\right), \tag{2.6}$$

$$-2\epsilon\widetilde{\boldsymbol{\nabla}}^2\widetilde{\phi}=\widetilde{c}^{+}-\widetilde{c}^{-}, \tag{2.7}$$

$$\widetilde{\boldsymbol{\nabla}}\cdot\widetilde{\boldsymbol{u}}=0, \tag{2.8}$$

$$\frac{1}{\mathrm{Sc}}\frac{\partial \widetilde{\boldsymbol{u}}}{\partial \widetilde{t}}=-\widetilde{\boldsymbol{\nabla}}\widetilde{p}+\widetilde{\boldsymbol{\nabla}}^2\widetilde{\boldsymbol{u}}-\frac{\kappa}{2\epsilon^2}(\widetilde{c}^{+}-\widetilde{c}^{-})\widetilde{\boldsymbol{\nabla}}\widetilde{\phi}, \tag{2.9}$$

where each tilde denotes a variable nondimensionalized by the above reference quantities.

For typical aqueous systems, $\kappa=0.5$ and $\mathrm{Sc}=1000$ are used. The nondimensional Debye screening length is assumed to be $\epsilon=10^{-3}$ (Druzgalski *et al.* 2013; Davidson *et al.* 2016). Our preliminary studies have shown that $\Delta V=180$ can be sufficient to develop electroconvective instability, although smaller voltages also show similar (but less significant) instability. While those parameters are fixed in their value, the AC frequency and diffusivity ratio are systematically varied to characterize the onset of electroconvective instability. The oscillation frequency is scaled by the intrinsic RC timescale of the equivalent circuit model, $\tau_{\mathrm{c}}=\lambda_{\mathrm{D}}L/D^+$ (Bazant *et al.* 2004; Olesen *et al.* 2010). Thus, $\omega/(2\pi)=\epsilon^{-1}$ corresponds to the dimensionless RC charging frequency. For the diffusivity ratio, cation diffusivity is used as reference, and anion diffusivity is varied.

The simulation domain is periodic in the x_1 direction with length $2\pi L$. On the electrode surface at $x_2/L=0$ and 1, the no-slip condition is used for fluid velocity, and ion fluxes normal to the surfaces are set to zero. For electric potential, the top wall is grounded, and the bottom wall has an externally imposed sinusoidal voltage $\Delta V\cos(\omega\widetilde{t})$, where ω is the dimensionless angular frequency. The phase angle θ is also used to describe the AC voltage oscillation; for example, $\theta=0$ corresponds to the bottom electrode having the maximum positive voltage $V_{\max}$, while $\theta=\pi$ corresponds to $\phi(y/L=0)=-V_{\max}$.

At $t = 0$, ionic conentrations are unity for both species, and fluid velocities are zero everywhere. Initial random disturbances are imposed on $c^{\pm}(t = 0)$ with the maximum perturbation being $5 \times 10^{-12} c_0$. Preliminary studies have shown that the perturbation magnitude does not have a meaningful influence on electroconvective instability after the first few oscillation periods for which initial transient effects are still non-negligible.

3. Numerical methods

The nondimensional governing equations, Eqs. (2.6)-(2.9), are solved using the numerical scheme introduced by Karatay *et al.* (2015) with the modification of Davidson (2017) to enforce discrete conservation at all iteration levels. The simulation domain is decomposed into a number of Cartesian control volumes, and some variables are staggered so that velocities and ion fluxes are defined at face centers, while the other variables are located at cell centers. The governing equations are integrated over control volumes and discretized with second-order accuracy in space. For numerical stability, simple averaging is used to compute face-centered quantities, instead of accounting for nonuniform grid spacing.

The presence of very thin EDLs near electrode surfaces renders the system of discretized equations numerically stiff, requiring a prohibitively small computational time step size. This difficulty is alleviated by using a semi-implicit treatment of fluxes in the wall-normal direction. The second-order backward Euler method is used for temporal discretization. At each time step, nonlinear terms are linearized, and the system of linearized governing equations is iteratively solved until they converge. Karatay *et al.* (2015) expanded electromigration fluxes using the product rule and simplified, which is a reasonable assumption for a reservoir–membrane setup under moderate applied DC voltage. However, the present configuration, where a much higher voltage is applied to a closed electrokinetic system, is more prone to numerical instability in a long time limit, if such non-conservative treatment is retained. Also, if a chemical reaction is allowed to occur, the importance of a fully conservative treatment is even more pronounced for numerical stability and accuracy (Pitsch 2006). Thus, electromigration flux is kept in the conservative form, which requires solving the linearized Nernst–Planck equations simultaneously with the linearized Poisson equation, increasing the size of the system matrix 1.5 times in each direction. However, this renders the overall algorithm fully conservative and enhances numerical stability.

The computational grid in the periodic x_1 direction is uniform in spacing. In the wall-normal x_2 direction, a hyperbolic tangent profile is used to create nonuniformly spaced grid points clustered near the electrodes. Grid spacings in the x_2 direction are symmetric with respect to $x_2/L = 0.5$. In the x_1 and x_2 directions, respectively, 1024 and 200 control volumes are used. Uniform grid spacing Δx_1 corresponds to $6\lambda_D$. In the x_2 direction, approximately 13 cells are used to resolve the EDL, and the minimum and maximum grid spacings are $\Delta x_{2,\min} = 0.05\lambda_D$ and $\Delta x_{2,\max} = 0.018L$, respectively.

Computational time step size is kept constant as $\Delta t D^+/L^2 = 10^{-7}$. This corresponds to 10^4 time steps per oscillation period at the highest AC frequency considered in this study, $\omega/(2\pi) = \epsilon^{-1}$. The number of iterations per time step ranges from 2 to 10, primarily depending on applied voltage and diffusivity ratio. An L_∞-error tolerance is prescribed to be 10^{-3} for convergence. Simulations are time advanced for 10 oscillation periods, after which statistics are collected for another 10 periods.

The simulation code has been verified by using the manufactured solution method and

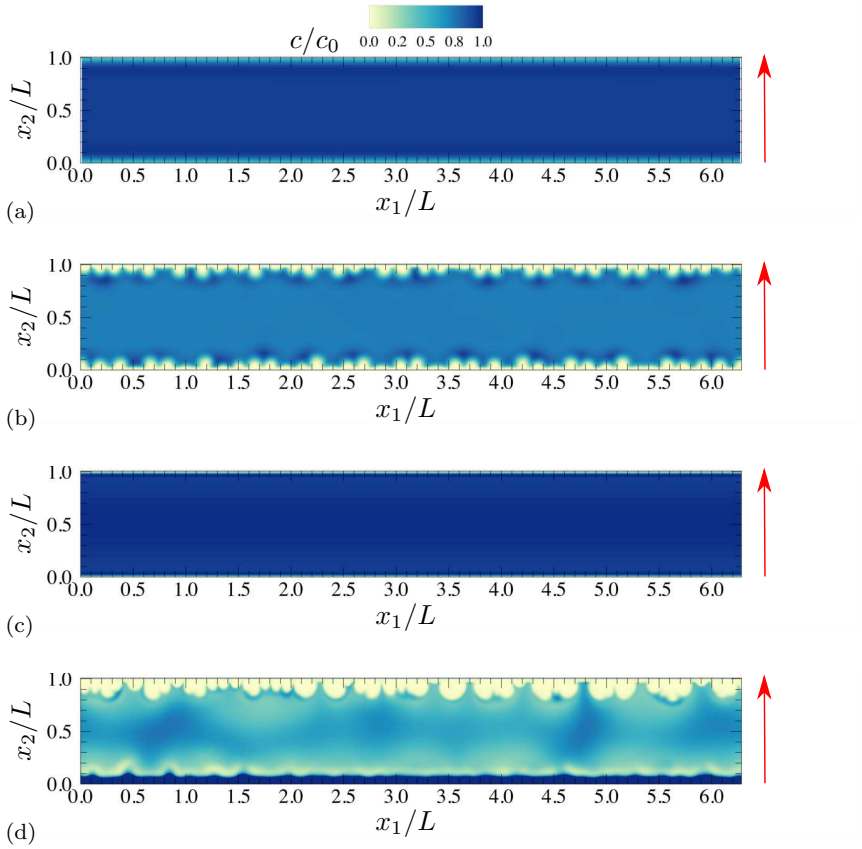

FIGURE 2. Instantaneous contours of salt concentration at $\theta = 2\pi/5$ for (a) $\Delta V = 40$, $\omega/(2\pi) = 0.1\epsilon^{-1}$, $D^-/D^+ = 1$, (b) $\Delta V = 180$, $\omega/(2\pi) = 0.1\epsilon^{-1}$, $D^-/D^+ = 1$, (c) $\Delta V = 180$, $\omega/(2\pi) = \epsilon^{-1}$, $D^-/D^+ = 1$ and (d) $\Delta V = 180$, $\omega/(2\pi) = \epsilon^{-1}$, $D^-/D^+ = 50$. The vertical arrows denote the direction of the applied electric field.

by comparing with asymptotic solutions of a symmetric binary mixture in contact with a cation-selective membrane under applied DC voltages.

4. Results

4.1. *Onset of electroconvective instability: the role of frequency and diffusivity ratio*

Under AC voltages, the electrohydrodynamic coupling term in Eq. (2.9) periodically changes its sign. Thus, compared to the same magnitude DC voltage, it is relatively difficult to induce electroconvective instability under AC voltages. This is even more pronounced at higher oscillation frequencies, where there is little or no time for hydrodynamic fluctuations to grow and attain finite amplitudes before they are damped by the action of reversed electric fields. This implies that high AC voltages (in units of thermal volts) at frequencies comparable to or smaller than the inverse of characteristic flow timescale are desired for the onset of electroconvective instability. Figure 2(a) illustrates this scenario. At $\Delta V = 40$, where some electroconvective instability is reported under the DC configuration (Druzgalski *et al.* 2013), no sign of instability is observed. Rather,

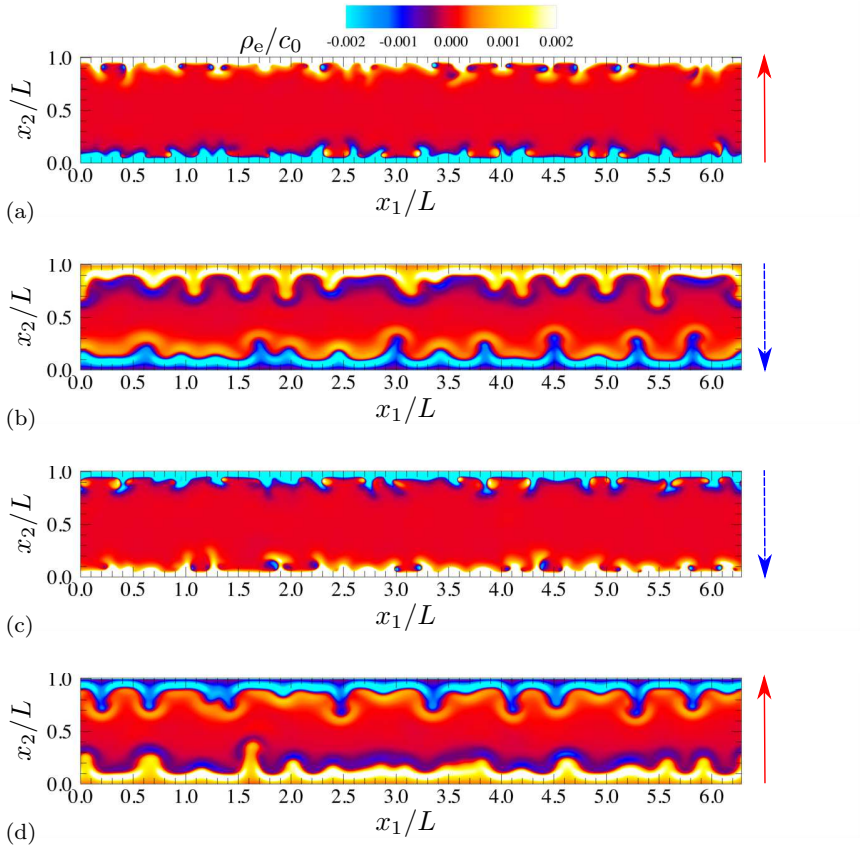

FIGURE 3. Instantaneous contours of charge density for $\omega/(2\pi) = 0.05\epsilon^{-1}$ at (a) $\theta = 0.36\pi$, (b) 0.88π, (c) 1.36π and (d) 1.88π. The diffusivity ratio is unity, and $\Delta V = 180$. The vertical arrows denote the direction of the applied electric field.

the electrolyte is nearly uniform in salt concentration and charge neutral. A comparison to the corresponding solution of the one-dimensional Nernst–Planck models (not shown in this report) confirms that the system is essentially one dimensional. However, a higher applied voltage, $\Delta V = 180$, at the same frequency induces strong transverse gradients of concentration and organized structures penetrating into the electroneutral bulk region with some characteristic length scales, as can be seen in Figure 2(b). At the same applied voltage, $\Delta V = 180$, however, a higher oscillation frequency at $\omega/(2\pi) = \epsilon^{-1}$ completely suppresses the instability, as shown in Figure 2(c). In addition to voltage and frequency, asymmetry in ion diffusivity has substantial impacts on the development of instability. Figure 2(d) shows that increasing the diffusivity ratio by a factor of 50 enhances electroconvective instability dramatically. Extended regions of ion depletion and enrichment are observed near electrodes. Also, structures near the two electrodes as well as in the bulk region are asymmetric and more irregular compared to those with equal diffusivities in Figure 2(b). Abu-Rjal *et al.* (2017) reported similar results in a DC membrane setup. For the remainder of this report, the maximum voltage is fixed at $\Delta V = 180$, and the effects of oscillation frequency and diffusivity ratio are examined. Figure 3(a)-(d) shows the time series of charge density at several phases of applied AC voltages spaced by $\Delta\theta = \pi/2$.

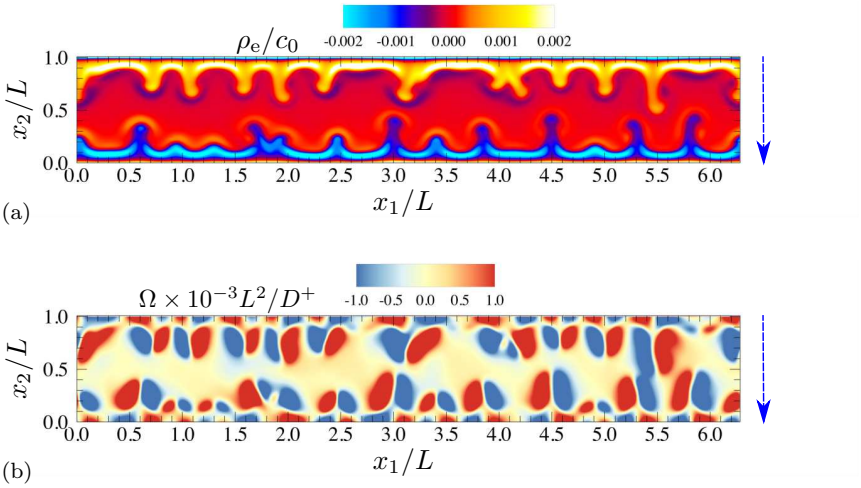

FIGURE 4. Instantaneous contours of (a) charge density and (b) vorticity at $\theta = 0.96\pi$ for $D^-/D^+ = 1$, $\omega/(2\pi) = 0.05\epsilon^{-1}$ and $\Delta V = 180$. The vertical arrows denote the direction of the applied electric field.

The diffusivity ratio is unity, and the oscillation frequency is $\omega/(2\pi) = 0.05\epsilon^{-1}$. In this configuration, electroconvective instability starts to develop at $\omega/(2\pi) \lesssim 0.1\epsilon^{-1}$. Note that in Figure 3(a,d) the bottom electrodes are cathodes, while in Figure 3(b,c) they are anodes. As the bottom electrode switches from positive [Figure 3(a)] to negative potential [Figure 3(b)] – or negative to positive between Figure 3(c,d) –, electromigration occurs primarily in the wall-normal direction, accompanied by the formation of finger-like structures. As demonstrated in Figure 4(b), such structures are created by pairs of counter-rotating vortices aligned near electrodes. As a result, large-scale mixing and ion transport from electrode surfaces to the bulk electrolyte are significantly enhanced.

Similar observations can be made for $D^-/D^+ = 10$ at the same frequency. However, increased anion diffusivity (and thus higher anion mobility) causes strong asymmetry and much less organized structures even in the bulk fluid zone. Their growth and abrupt collapse involve intense hydrodynamic mixing. This is particularly the case for phases after the applied electric field changes its sign, as demonstrated in Figure 5(b,d). Compared to Figure 4(a), where the primary direction of electroconvection is wall normal, significant transverse motions are observed.

When electroconvective instability occurs, limit-cycle oscillations are quickly established in the first few oscillation periods. Typically, the maximum induced velocity magnitude over the entire volume becomes considerably larger than the diffusion velocity D^+/L, since convective transport becomes significant. For the case of equal diffusivity, electroconvective instability begins to appear at $\omega/(2\pi) \lesssim 0.1\epsilon^{-1}$. As shown in Figure 6(a), the maximum magnitude of u_1 ranges from $O(10^2)$ to $O(10^3)$ of diffusion velocity at $\omega/(2\pi) = 0.1\epsilon^{-1}$, where electroconvective instability is observed. At higher frequencies, shown in Figure 6(a), the system remains stable, and the maximum induced velocity is lower than the diffusion velocity.

At a fixed frequency, the maximum horizontal velocity increases with respect to the diffusivity ratio, as shown in Figure 6(b). Periodic orbits corresponding to nonequal diffusivity are more irregular and secondary branches are derived, suggesting that their

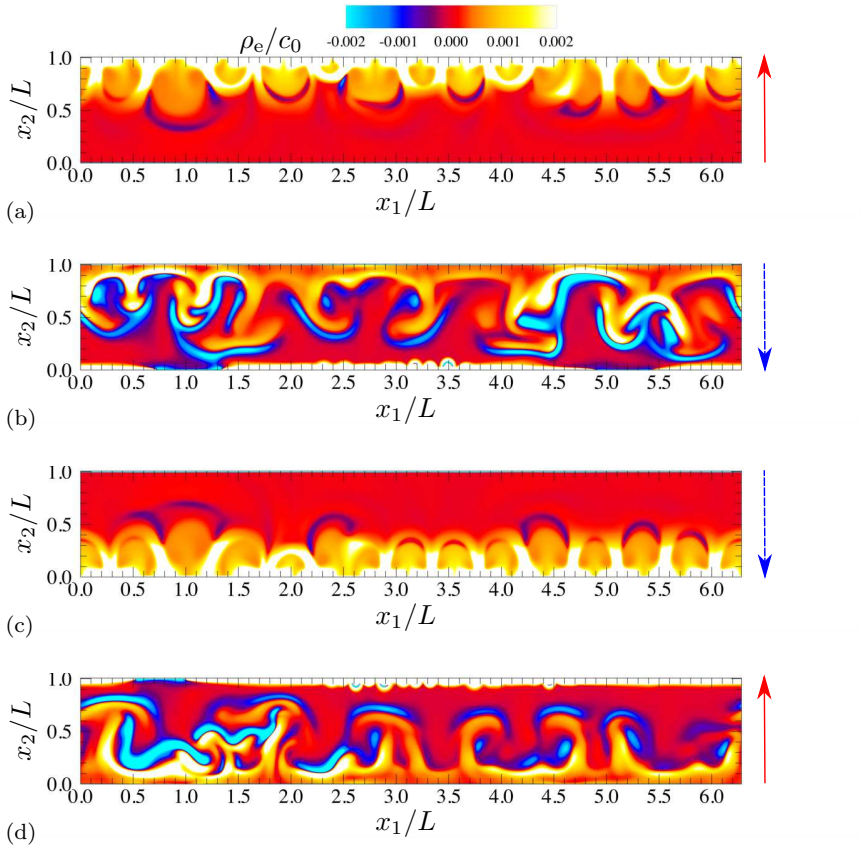

FIGURE 5. Instantaneous contours of charge density for $\omega/(2\pi) = 0.05\epsilon^{-1}$ at (a) $\theta = 0.28\pi$, (b) 0.8π, (c) 1.28π and (d) 1.8π. Diffusivity ratio is $D^-/D^+ = 10$, and $\Delta V = 180$. The vertical arrows denote the direction of the applied electric field.

underlying instability mechanisms are more complex and presumably more chaotic, as evidenced by Figure 5.

4.2. *Characterization of electroconvective instability*

Observations so far have shown that the onset of electroconvective instability is a strong function of applied AC voltage magnitude, oscillation frequency and diffusivity ratio of ionic species. To characterize its dynamics, it is useful to introduce a quantitative measure for electroconvective instability. In this study, the maximum transverse velocity magnitude $u_{1,\max}$ is employed, among many others.

Figure 7 shows the maximum induced velocities in the electrolyte for 10 oscillation periods. For nonequal diffusivities, the maximum velocities take their peak values at $\omega/(2\pi) = 0.1\epsilon^{-1}$ for both u_1 and u_2, and responses at higher frequencies diminishes monotonically. For equal diffusivity, appreciable electrohydrodynamic responses begin to appear at $\omega/(2\pi) \leq 0.1\epsilon^{-1}$. It is likely that a similar peak exists for equal diffusivity at a frequency equal to or lower than $\omega/(2\pi) = 0.02\epsilon^{-1}$. Additional simulations are under way to address this question.

As shown in Figure 5, strong electroconvective instability significantly enhances trans-

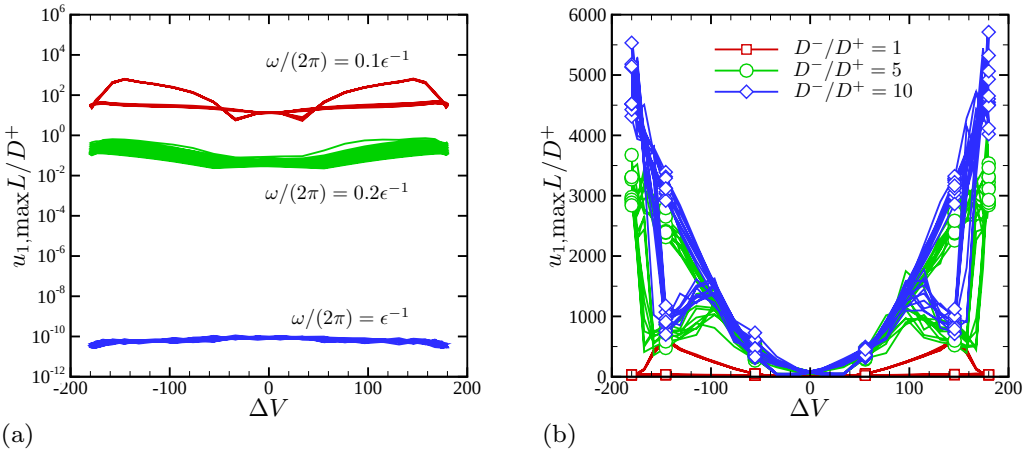

FIGURE 6. Trajectories of maximum horizontal velocity $u_{1,\max}$ for 10 oscillation periods. Each curve corresponds to a different (a) oscillation frequency for $D^-/D^+ = 1$ and (b) diffusivity ratio at $\omega/(2\pi) = 0.1\epsilon^{-1}$.

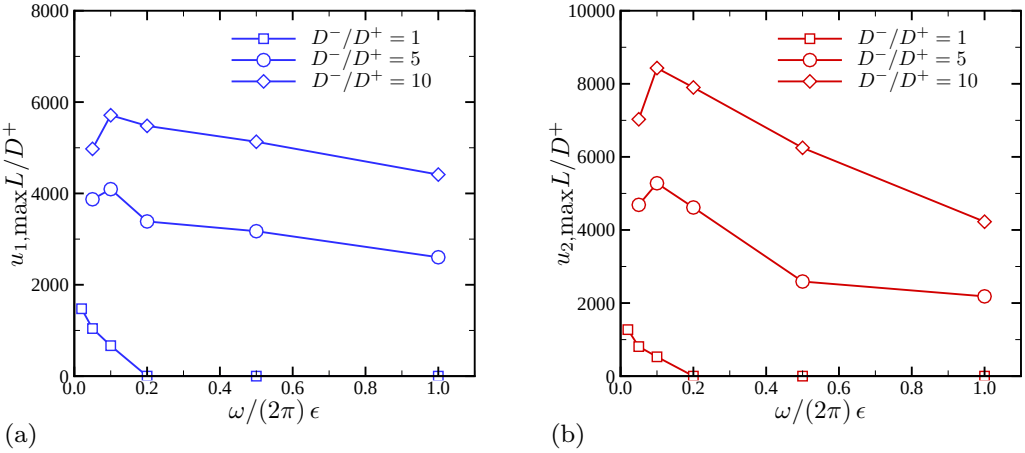

FIGURE 7. Maximum velocities in the (a) transverse and (b) wall-normal directions for 10 oscillation periods.

port of ionic species. Figure 8(a) shows salt concentration averaged over time and in the x_1 direction. Due to symmetry, only $0 \leq x_2/L \leq 0.5$ is shown. Compared to the case with equal diffusivity and $\omega/(2\pi) = 0.1\epsilon^{-1}$ (solid line), where electroconvective instability is mild [Figures 6(b) and 7], nonequal diffusivity significantly modifies the wall-normal distribution of salt. At $\omega/(2\pi) = 0.1\epsilon^{-1}$ (dashed line), where $u_{1,\max}$ is optimal for $D^-/D^+ = 10$, excess salt concentration is observed at $x/L \lesssim 0.1$, while mean bulk concentration is reduced by a factor of three. This suggests that electroconvective instability functions as efficient transport mechanisms by, on average, pumping bulk ionic species toward the electrode. An order-of-magnitude-higher wall-normal velocity fluctuation in the bulk region (dashed line) in Figure 8(b) also supports such mechanisms. As frequency increases to $\omega/(2\pi) = \epsilon^{-1}$ (dashed-dotted line), the instability becomes less

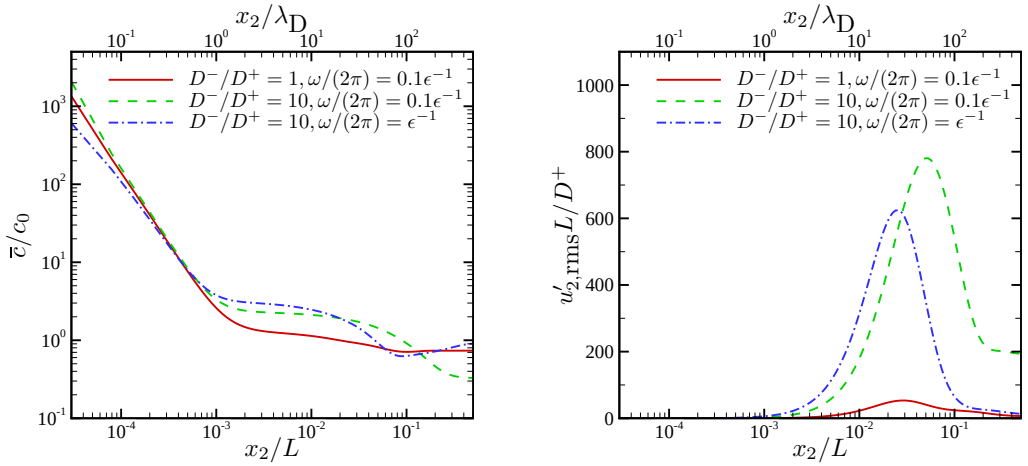

FIGURE 8. (a) Mean salt concentration and (b) root-mean-square (rms) fluctuations of wall-normal velocity u_2.

strong, and the bulk concentration recovers the value of the quiescent electrolyte ($c_0 = 1$). Also, the impact of electroconvection is more or less restricted for $\epsilon \lesssim x_2/L \lesssim 0.1$.

5. Conclusions

An aqueous electrolyte under applied AC voltages is simulated and analyzed for electroconvective instability, previously reported and studied by Druzgalski *et al.* (2013) and Davidson *et al.* (2016) under DC electric fields. The governing two-dimensional Poisson–Nernst–Planck equations coupled with Navier–Stokes equations at the incompressible, low-Reynolds limit are directly solved using a fully conservative, time-implicit numerical scheme based on that of Karatay *et al.* (2015). Under certain conditions where sufficiently strong AC voltages are applied, electroconvective instability is developed and sustained. The formation and breakdown of pairs of counter-rotating vortices near electrodes promote large-scale transport of ionic species and hydrodynamic mixing. Two important parameters, namely AC oscillation frequency ω and the ratio of diffusivity D^-/D^+, are assessed for their impacts on electroconvective instability. When measured by the maximum transverse velocity, the instability is a strong function of those two parameters. In general, a lower oscillation frequency and a higher diffusivity ratio are more useful to trigger and sustain the instability. For nonequal diffusivities, electroconvective instability is observed for all oscillation frequencies (up to the intrinsic RC frequency) examined in this study. States of optimal frequency responses are identified at a frequency 10 times lower than the RC frequency of the electrolyte. At $D^-/D^+ = 1$, electroconvective instability develops at $\omega/(2\pi) \lesssim 0.1\epsilon^{-1}$.

Extensions of the present work include more detailed characterization of electroconvective instability using other types of measures, reduced-order models for near-wall structures and their stability characteristics. Additionally, a stability diagram of the given electrokinetic system will be developed to completely characterize the system behavior under AC voltages. This will require additional parametric studies for oscillation frequency, diffusivity ratio and applied voltage. In particular, much larger voltages,

$O(10^3)$ to $O(10^4)$ thermal volts, are of interest. Also, diffusivity ratios much higher than $D^-/D^+ = 10$ (say, 10^2 or 10^3) will be investigated. These conditions are inspired mainly for applications of plasma discharge, which will also require inclusion of chemical reaction, thermal nonequilibrium (by solving an energy equation) and variable transport properties such as dynamic viscosity and ionic diffusivity as a function of local temperature. In particular, stronger applied voltage and severe asymmetry in ion diffusivity pose considerable challenges to the numerical stability of the predictions. However, if the gas phase is simulated, the electrohydrodynamic coupling constant becomes significantly smaller ($\approx 2 \times 10^{-5}$) than $\kappa = 0.5$ for water. This effectively reduces the Courant number of time advancement when the same magnitude voltage is applied. Also, the Debye screening length for a gas is typically an order of magnitude larger, thereby alleviating the numerical stiffness of the system matrices.

Acknowledgments

This work is supported by the Stanford Precourt Institute for Energy.

REFERENCES

Abu-Rjal, R., Prigozhin, L., Rubinstein, I. & Zaltzman, B. 2017 Equilibrium electro-convective instability in concentration polarization: The effect of non-equal ionic diffusivities and longitudinal flow. *Russ. J. Electrochem.* **53**, 903–918.

Bazant, M. Z., Thornton, K. & Ajdari, A. 2004 Diffuse-charge dynamics in electrochemical systems. *Phys. Rev. E* **70**, 021506.

Chang, H.-C., Yossifon, G. & Demekhin, E. A. 2012 Nanoscale electrokinetics and microvortices: How microhydrodynamics affects nanofluidic ion flux. *Annu. Rev. Fluid Mech.* **44**, 401–426.

Davidson, S. M., Andersen, M. B. & Mani, A. 2014 Chaotic induced-charge electro-osmosis. *Phys. Rev. Lett.* **112**, 128302.

Davidson, S. M., Wessling, M. & Mani, A. 2016 On the dynamical regimes of pattern-accelerated electroconvection. *Sci. Rep.* **6**, 22505.

Davidson, S. M 2017 A comprehensive investigation of electroconvection in canonical electrochemical environments. PhD Thesis, Stanford University.

Demekhin, E. A., Nikitin, N. V. & Shelistov, V. S. 2013 Direct numerical simulation of electrokinetic instability and transition to chaotic motion. *Phys. Fluids* **25**, 122001.

Demekhin, E. A., Shelistov, V. S. & Polyanskikh, S. V. 2011 Linear and nonlinear evolution and diffusion layer selection in electrokinetic instability. *Phys. Rev. E* **84**, 036318.

Druzgalski, C. & Mani, A. 2016 Statistical analysis of electroconvection near an ion-selective membrane in the highly chaotic regime. *Phys. Rev. Fluids* **1**, 073601.

Druzgalski, C. L., Andersen, M. B. & Mani, A. 2013 Direct numerical simulation of electroconvective instability and hydrodynamic chaos near an ion-selective surface. *Phys. Fluids* **25**, 110804.

Karatay, E., Druzgalski, C. L. & Mani, A. 2015 Simulation of chaotic electrokinetic transport: Performance of commercial software versus custom-built direct numerical simulation codes. *J. Colloid Interf. Sci.* **446**, 67–76.

Nikonenko, V. V., Kovalenko, A. V., Urtenov, M. K., Pismenskaya, N. D.,

Han, J., Sistat, P. & Pourcelly, G. 2014 Desalination at overlimiting currents: State-of-the-art and perspectives. *Desalination* **342**, 85–106.

Nikonenko, V. V., Mareev, S. A., Pismenskaya, N. D., Uzdenova, A. M., Kovalenko, A. V., Urtenov, M. K. & Pourcelly, G. 2017 Effect of electroconvection and its use in intensifying the mass transfer in electrodialysis. *Russ. J. Electrochem.* **53**, 1122–1144.

Nikonenko, V. V., Vasil'eva, V. I., Akberova, E. M., Uzdenova, A. M., Urtenov, M. K., Kovalenko, A. V., Pismenskaya, N. P., Mareev, S. A. & Pourcelly, G. 2016 Competition between diffusion and electroconvection at an ion-selective surface in intensive current regimes. *Adv. Colloid Interfac.* **235**, 233–246.

Olesen, L. H., Bazant, M. Z. & Bruus, H. 2010 Strongly nonlinear dynamics of electrolytes in large ac voltages. *Phys. Rev. E* **82**, 011501.

Pham, V. S., Li, Z., Lim, K. M., White, J. K. & Han, J. 2012 Direct numerical simulation of electroconvective instability and hysteretic current-voltage response of a permselective membrane. *Phys. Rev. E* **86**, 046310.

Pitsch, H. 2006 Large-eddy simulation of turbulent combustion. *Annu. Rev. Fluid Mech.* **38**, 453–482.

Rubinstein, I., Staude, E. & Kedem, O. 1988 Role of the membrane surface in concentration polarization at ion-exchange membrane. *Desalination* **69**, 101–114.

Rubinstein, S. M., Manukyan, G., Staicu, A., Rubinstein, I., Zaltzman, B., Lammertink, R. G., Mugele, F. & Wessling, M. 2008 Direct observation of a nonequilibrium electro-osmotic instability. *Phys. Rev. Lett.* **101**, 236101.

Schnitzer, O. & Yariv, E. 2014 Nonlinear oscillations in an electrolyte solution under ac voltage. *Phys. Rev. E* **89**, 032302.

Stout, R. F. & Khair, A. S. 2015 Moderately nonlinear diffuse-charge dynamics under an ac voltage. *Phys. Rev. E* **92**, 032305.

Suh, Y. K. & Kang, S. 2008 Asymptotic analysis of ion transport in a nonlinear regime around polarized electrodes under ac. *Phys. Rev. E* **77**, 031504.

de Valença, J. C., Wagterveld, R. M., Lammertink, R. G. H. & Tsai, P. A. 2015 Dynamics of microvortices induced by ion concentration polarization. *Phys. Rev. E* **92**, 031003.

Zaltzman, B. & Rubinstein, I. 2007 Electro-osmotic slip and electroconvective instability. *J. Fluid Mech.* **579**, 173–226.